JBC Papers in Press. Published on January 12, 2020 as Manuscript RA119.011536
The latest version is at http://www.jbc.org/cgi/doi/10.1074/jbc.RA119.011536

Analyses of the oncogenic BRAF^{D594G} variant reveal a kinase-independent function of BRAF in activating MAPK signaling

Nicholas J. Cope, Borna Novak, Zhiwei Liu, Maria Cavallo, Amber Y. Gunderwala, Matthew Connolly, Zhihong Wang*

Department of Chemistry & Biochemistry, University of the Sciences, Philadelphia, PA 19104, United States

Running title: Oncogenic BRAF^{D594G} reveals kinase-independent function

*Correspondence (Z.W.) Telephone: (215) 596-7082 Email: z.wang@usciences.edu

Keywords: DFG motif, RAF kinase, autophosphorylation, molecular dynamics, paradoxical activation, 14-3-3 protein, peptide inhibitor, allosteric activation, cancer, kinase signaling

Abstract

Class 3 mutations in *B-Raf* proto-oncogene, Ser/Thr kinase (BRAF) that result in kinase-impaired or kinase-dead BRAF have the highest mutation frequency in *BRAF* gene in lung adenocarcinoma. Several studies reported that kinase-dead BRAF variants amplify Mitogen-Activated Protein Kinase (MAPK) signaling by dimerizing with and activating wild-type *C-Raf* proto-oncogene, Ser/Thr kinase (CRAF). However, the structural and functional principles underlying their activation remain elusive. Herein, using cell biology and various biochemical approaches, we established that variant BRAF^{D594G}, a kinase-dead representative of class 3 mutation-derived BRAF variants, has a higher dimerization potential as compared to wild-type BRAF. Molecular dynamics simulations uncovered that the D594G substitution orients the αC-helix toward the IN position and extends the activation loop within the kinase domain, shifting the equilibrium towards the active, dimeric conformation, thus priming BRAF^{D594G} as an effective allosteric activator of CRAF. We found that B/CRAF heterodimers are the most thermodynamically stable RAF dimers, suggesting that RAF heterodimers, and not homodimers, are the major player in determining the amplitude of MAPK signaling in cells. Additionally, we show that BRAF^{D594G}:CRAF heterodimers bypass autoinhibitory P-loop phosphorylation, which might contribute to longer duration of MAPK pathway signaling in cancer cells. Lastly, we propose that the dimer interface of BRAF^{D594G}:CRAF heterodimer may represent a promising target in the design of novel anticancer therapeutics.

Introduction

The MAPK, Mitogen-Activated Protein Kinase, pathway is important in regulating cell proliferation and survival. Duration and amplitude of MAPK signaling is mainly controlled by the RAF Ser/Thr kinase family: ARAF, BRAF, and CRAF, which contain three conserved regions (CR) for membrane recruitment (CR1), N-terminal 14-3-3 regulation (CR2), and catalysis (CR3).(1) Among the three RAF isoforms, BRAF has the highest basal activity and is most frequently mutated in 7-8% of all human cancers.(2) The high mutation propensity in cancer led to extensive interest in the development of BRAF-specific drugs.

Wild-type (WT) BRAF requires RAS-initiated membrane recruitment and homo- or hetero-dimerization with other RAF isoforms for activation. Although all BRAF mutations trigger constitutive activation of MAPK signaling in cancer cells, they have distinct activation mechanisms and have been grouped into three main classes to reflect different biochemical properties: RAS and dimer independent (class 1), RAS independent but dimer dependent (class 2), and RAS and dimer dependent (class 3).(3) Class 1 mutations include the most common BRAF mutation V600E that accounts for ~90% of all BRAF mutations.(2) The prominence of BRAF^{V600E} led to FDA approval of two ATP-competitive drugs

vemurafenib and dabrafenib.(4) These ATP-competitive drugs elicit effective clinical outcomes for melanoma patients carrying the V600E mutation; however, paradoxical activation and drug resistance restrict their application to cancers driven by class 2 and 3 BRAF mutations.(3,5,6)

Inactivating BRAF mutations, class 3, are currently the most common BRAF mutation in lung adenocarcinoma.(7) Herein, we study a representative of class 3 BRAF mutations, BRAF^{D594G}, which is the most frequent kinase-dead mutation. D594 is part of the highly conserved DFG motif found in all kinases. The aliphatic residues Phe/Gly help to maintain the closed inactive conformation by occupying the ATP binding pocket, while the Asp residue is a key catalytic residue involved in Mg^{2+} coordination for the phospho-transfer reaction. Therefore, the mutation of D594 to Gly prevents Mg^{2+} coordination, rendering BRAF catalytically inactive.

Intriguingly, the 'kinase-dead' BRAF mutation has been validated as a driver of lung carcinoma,(8,9) suggesting that BRAF has functions that are not limited to catalyzing MEK phosphorylation but extend to other roles that are independent of enzyme activity. In parallel, the FDA-approved BRAF inhibitors inhibit the catalytic activity of wild-type BRAF while boosting the non-catalytic function of BRAF to further upregulate the MAPK signaling, which leads to secondary malignancies in clinic.(5,6,10) This phenomenon, known as 'paradoxical activation', is a major concern surrounding current BRAF inhibitors. Apparently, ATP-competitive inhibitors rearrange the structural elements of BRAF kinase to augment the non-catalytic functions, resulting in fundamentally different biological outcomes. Our current view of RAF regulation is mainly derived from mechanistic studies of enzymatically active RAF kinases by evaluating their catalytic capability. The biochemistry of non-catalytic BRAF functions is poorly understood.

The unknown non-catalytic behavior of BRAF generates therapeutic limitations of ATP-competitive RAF drugs, including paradoxical activation and drug resistance. It remains a challenge to directly target kinase-dead BRAF mutants with traditional ATP-competitive inhibitors. Novel approaches are in urgent need. Here we integrate biophysical, biochemical, and computational approaches together with cellular assays to explore the non-catalytic function of BRAF in cancer. Additionally, our study sheds light on the activation and regulation mechanism of RAF kinase family under physiological and pharmacological conditions.

Results

BRAF^{D594G} is More Prone to Dimerization than WT BRAF- Dimerization through the kinase domain is required for WT BRAF and non-V600 BRAF mutations to function in normal and cancerous cells.(8,11) Previously, Heidorn *et al.* have shown that kinase-dead BRAF^{D594A} dimerizes with CRAF when transiently transfected into D04 NRAS^{Q61L} cancer cells,(12) and Yao *et al.* determined that BRAF^{D594G} has a stronger binding potential than WT BRAF to RAS.(8) To complement the previous cellular studies, we examined how this mutation affects the biochemical properties of BRAF in its purified form. Thus, we purified the catalytic domain (CD) of BRAF^{D594G} from *E. coli* through affinity and size exclusion chromatography with a purity of >90% suitable for biophysical analyses (Figure 1A). CD-BRAF^{D594G} was subjected to velocity analytical ultracentrifugation (AUC) to determine the mass of macromolecules in solution. The majority of our protein sedimented with a sedimentation coefficient (S) of ~ 3.8 S, which relates to dimeric BRAF previously identified by Grasso *et al.* (Figure. 1B).(13) WT CD-BRAF and a small population of CD-BRAF^{D594G} exist at ~2.6 S, which relates to monomeric BRAF, previously identified by our lab and others (Figure 1B).(13-15)

Next, we conducted molecular dynamics (MD) simulations on monomeric and dimeric WT BRAF and monomeric BRAF^{D594G} to elucidate the structural basis for enhanced dimerization. The starting structures are WT monomeric (PDB:4WO5(14) and dimeric (PDB:4E26(16)) kinase domain, respectively. The BRAF^{D594G} initial structure is constructed by mutating the WT monomer crystal structure (PDB:4WO5(14). The inhibitors in the crystal structure were removed. We did not include ATP molecules, because BRAF^{D594G} mutation disables ATP-binding (Figure S1). One hallmark of BRAF activation is the movement of the αC-helix, with respect to orientation towards the C-lobe, from OUT

(inactive) to IN (active) conformation. The production runs of the simulations were carried out for 200-400 ns. The distances between the center of masses of the αC-helix and the C-lobe were measured as on average 30 ± 0.44 Å, 28.5 ± 0.45 Å, 25.6 ± 0.30 Å, for monomeric BRAF^{WT}, monomeric BRAF^{D594G}, and dimeric BRAF^{WT}, respectively. This emphasizes that the αC-helix of monomeric BRAF^{D594G} is closer to the C-lobe than the monomeric WT counterpart (Figure 1C&D). In the αC-helix-IN conformation, residues in the αC-helix stabilize RAF dimers through hydrophobic interactions (R509 with W450) and H-bonds (R509 with T508/R506/L505). Our previous MD simulations together with structures of monomeric BRAF kinase domain support that a fully-extended activation loop stabilizes active BRAF while a rigid secondary-structure element, termed helix AS-H1, maintains an inactive conformation of BRAF.(14,17) The possibility of forming secondary structures, including 3_{10} helix and α-helix, were summarized in Table 1. The MD simulations show that the activation loop of BRAF^{D594G} is in a transition between the AS-H1 and extended loop, which is supported by the loss of the α-helical structure of the activation loop, while aa.598-600 form a short 3_{10} helix (Figure 1D&E; Table 1). The formation of the 3_{10} helix is a product of the torsional strain placed on the N-terminal of the activation loop as the C-terminal unwinds.

Together, these observations support that monomeric CD-BRAF^{D594G} adopts a partially active conformation indicating higher dimerization potential than CD-BRAF^{WT} as demonstrated by the AUC data (Figure 1D). Additionally, adopting the partially activated state instead of fully activated state minimizes BRAF^{D594G} homo-dimerization which occurs when the αC-helix and activation loop are fully IN and extended, as evidenced by oncogenic BRAF^{V600E}.(17)

Dimerization Potential Correlates with the Kinase Activity of RAF Dimers- It was previously established that BRAF:CRAF heterodimers are the most active RAF dimers *in vitro*.(15) It remains elusive how this translates to ERK hyperactivation by BRAF^{D594G}:CRAF. In light of this, we transfected CRAF alone or co-transfected BRAF:CRAF or BRAF^{D594G}:CRAF into HEK293T cells and immunoprecipitated MBP-tagged CRAF using amylose resin to obtain either CRAF alone or BRAF:CRAF and BRAF^{D594G}:CRAF heterodimers, respectively. We added the MBP tag to enhance the solubility of CRAF for our *in vitro* experiments. The heterodimers have much higher activity than CRAF in cells and *in vitro* (Figure 2A&B). The activity of BRAF^{D594G}:CRAF is comparable to that of BRAF:CRAF. Thus, the kinase activity of BRAF is dispensable for transactivation of CRAF. Additionally, the observed high kinase activity rules out the possibility of forming stable RAF homodimers, as both BRAF^{D594G} and CRAF homodimers have no or very minimal kinase activity. This is consistent with our previous studies on BRAF:CRAF heterodimers, which demonstrated that separately purified BRAF and CRAF homodimers form stable BRAF:CRAF heterodimers after mixing *in vitro*.(15)

As mentioned previously, D594G is commonly found in lung cancer. To observe what effects lung cancer cells have on heterodimer activity, we performed a similar experiment in HTB-177 (KRAS^{Q61H}) lung cancer cells. For this experiment we transfected CRAF, D594G:CRAF, and BRAF:CRAF in HTB-177 cells and monitored their activity (Figure S2). As expected, BRAF^{D594G}:CRAF heterodimers activity is similar to that of BRAF:CRAF. This confirms that activity of BRAF is expendable for activation of CRAF. Additionally, the elevated activity in the presence of heterodimers establishes the necessary signaling output for transformation in cancer cells.

To understand why the BRAF:CRAF heterodimer forms readily, we applied MD simulations to investigate the atomistic details of BRAF:CRAF heterodimerization. We started with the dimeric CRAF (PDB:3OMV(6)) and dimeric BRAF ((PDB:4E26(16)) crystal structures with any bound inhibitors removed. The BRAF^{D594G}:CRAF heterodimer is constructed by replacing one protomer of the BRAF dimer with a CRAF protomer (extracted from the CRAF dimer structure) *via* alignment between the incoming and outgoing protomer, as well as introduction of D594G mutation to the remaining BRAF protomer. The production simulations of BRAF:BRAF, BRAF^{D594G}:CRAF, and CRAF:CRAF were carried out for 200 to 300 ns. By comparing the gain or loss and the strength of H-bonds, we conclude that BRAF:CRAF heterodimers are thermodynamically

more stable than the corresponding homodimers. The inter-protomer interaction can be illustrated by analyzing the distance between BRAF:CRAF R509/R401 (H-bond donors) to their corresponding H-bonding partners on the other protomer (Figure 2 C&D). The calculated distance (~3Å) for BRAF:CRAF and BRAF:CRAF dimers is ideal for H-bond formation between two protomers, but not for CRAF:CRAF dimer. In addition to the R509 H-bonds, BRAF^{D594G}:CRAF heterodimers have strong inter-protomer interactions between the following donor/acceptor pairs: H510/H369, H402/H477, and R398/D448. The average number of H-bonds (Table 2) is the sum of the fraction of H-bonds that occur in the simulations during a period of 150 to 200 ns. Thus, the BRAF^{D594G}:CRAF heterodimer forms the strongest dimer, followed by BRAF:BRAF, and CRAF:CRAF homodimer is the weakest of the three.

Together, the increased dimerization potential of the heterodimer is reflected by the increased BRAF:CRAF heterodimer activity *in cellulo* and *in vitro*. CRAF homodimer forms the weakest dimer, reinforcing the notion that CRAF has the lowest basal activity alone.

The Stability of* BRAF^{D594G}*:CRAF Heterodimers are 14-3-3 Dependent- The formation of BRAF:CRAF heterodimers occur in normal cells through RAS-induced membrane recruitment.(5,6,18,19) The factors promoting dimerization of oncogenic BRAF^{D594G}:CRAF remain controversial. In light of this, we created a series of BRAF^{D594G} truncation constructs: ΔN-tail (region containing the BRAF-specific region), ΔRAS-binding domain (ΔRBD), ΔCR2, and ΔSSDD by truncating from the N-terminal towards the kinase domain to identify which regions of BRAF^{D594G} are crucial for dimerization with CRAF (Figure 3A). We transiently transfected the BRAF^{D594G} deletion constructs: ΔN-tail, ΔRAS-binding domain (ΔRBD), ΔCR2, and ΔSSDD into HEK293 cells with or without WT CRAF. (Figure 3B). The BRAF^{D594G} constructs and CRAF have poor expression as single transfections, but when co-transfected together the expression increases on average 9- and 2-fold for BRAF^{D594G} and CRAF, respectively, suggesting that formation of BRAF^{D594G}:CRAF protects both proteins from degradation. The observed change in expression of both BRAF and CRAF can be used as a tool to determine whether heterodimer pairs form in cells. All of the BRAF^{D594G} constructs containing the SSDD motif were able to stabilize CRAF (Figure 3B). It is not surprising that ΔSSDD lost the ability to activate CRAF, as the SSDD motif is important for proper regulatory spine alignment which is a pre-requisite for dimerization and activation of RAF family members.(13)

14-3-3 chaperone protein binding to pS729 of BRAF enhances homo- or hetero-dimerization of WT RAF.(20,21) AMPK has been identified to phosphorylate the BRAF C-terminal 14-3-3 binding site, S729.(21) To verify the role of 14-3-3 on BRAF^{D594G}:CRAF dimerization, we treated cells expressing RAF heterodimers with Dorsomorphin 2HCl (Compound C), a potent AMPK inhibitor. The phosphorylation of Raptor, a well-established protein substrate of AMPK, was decreased in the presence of Compound C, verifying that AMPK is potently inhibited (Figure 3C). Additionally, total CRAF, pCRAF and pS729 were decreased in the context of BRAF^{D594G}:CRAF heterodimer (Figure 3C). To further verify the role of 14-3-3 binding, we introduced the S729A mutation to mimic unphosphorylated BRAF^{D594G}. Unfortunately, BRAF$^{D594G/S729A}$ was not expressed well in HEK293 cells, preventing more detailed investigation. This is consistent with Park and colleagues who show that the mutation to S729A results in poor stability of purified BRAF from insect or mammalian cells.(22) Regardless, the observed destabilization by the S729A mutation together with the compound C data suggest that 14-3-3 binding to pS729 stimulates BRAF^{D594G}:CRAF heterodimerization and subsequent CRAF activation. Since phosphorylation of S729 was not completely depleted by the AMPK inhibitor, these results suggest that there are other kinases, other than AMPK, that are responsible for S729 phosphorylation. In parallel, AMPK inhibitor has little effect on pS729 and pCRAF-S338 in the context of WT BRAF:CRAF heterodimers, suggesting that they have a distinct regulation mechanism.

BRAF^{D594G}:CRAF Heterodimers Bypass Autoinhibitory Phosphorylation in Cancer Cells- We previously identified that BRAF^{WT} can autophosphorylate it's P-loop (Ser465/Ser467) to inactivate itself in the absence of native substrate MEK.(15) By doing so, BRAF is subject to fine-

tuned regulation to ensure rapid termination of RAF signaling. To determine if BRAF:CRAF and BRAF^{D594G}:CRAF use a similar mechanism, we incubated these kinases with ATP for 30 min to let autophosphorylation complete prior to quantifying their specific activity. The activity of BRAF:CRAF was decreased by ~40-50% upon autophosphorylation (Figure 4A), suggesting that autophosphorylation of certain residues negatively regulates the kinase activity of BRAF. Intriguingly, no obvious change was detected for BRAF^{D594G}:CRAF (Figure 4A), demonstrating that oncogenic mutations can bypass autophosphorylation to sustain pathway signaling. To further verify this finding, we monitored total BRAF autophosphorylation via ^{32}P autoradiograph. As shown in Figure 4B, BRAF^{WT} was able to autophosphorylate itself and MEK; however, BRAF^{D594G}:CRAF could only phosphorylate BRAF^{D594G} and MEK, but not CRAF (Figure 4B). The lack of CRAF phosphorylation within BRAF^{D594G}:CRAF dimers provides compelling evidence that RAF autophosphorylation occurs in *trans*, not *cis*.

To further verify this model, we introduced the R509H mutation, a mutation known to disrupt the 'side-to-side' dimer interface of BRAF, to BRAF^{V600E}. As monomeric BRAF$^{V600E/R509H}$ is still active, our data clearly demonstrate that autophosphorylation requires an intact dimer interface and occurs as *trans*- rather than *cis*-autophosphorylation (Figure 4A&B). Our finding highlights the physiological significance of the 'side-to-side' dimer interface, other than allosteric *trans*-activation. Within a BRAF dimer, BRAF *trans*-phosphorylates both activation loop and inhibitory phosphorylation sites to fine-tune the overall BRAF activity (Figure 4A&B).(15,17)

P-loop Phosphorylation Destabilizes BRAF Dimers- Our mechanistic studies identified that P-loop phosphorylation negatively regulates the kinase activity of BRAF^{WT}.(17) We carried out MD simulations on dimeric BRAF^{WT} kinase domain with P-loop phosphorylation (pSer465/pSer467) and compared it with the simulations of WT unphosphorylated dimer. Both simulations started from the same crystal structure (PDB entry 4E26(16)). Our MD data demonstrate that phosphorylation of the P-loop disfavors dimer formation by disrupting multiple H-bonds in the dimer interface, whereas these H-bonds remained intact in the unphosphorylated dimer (Figure 4C). In addition, the two phosphorylated protomers also moved apart from each other (black trajectory, Figure 4C), relative to the unphosphorylated protomers (blue trajectory, Figure 4C), further validating the distorted dimer configuration. Other dimer simulations, including WT dimer and P-loop phosphorylation with inhibitors, and WT dimer with the R509H mutation, show consistent results of weakened dimeric interaction upon P-loop phosphorylation or introduction of the R509H mutation (Figure S3). Consistent with our MD simulations, co-immunoprecipitation experiments verified that introduction of phosphomimetic mutation S465D/S467D (SS/DD) to P-loop compromised the dimerization ability of BRAF, as shown in Figure 4D. Together, we conclude that P-loop phosphorylation decreases the formation of BRAF dimers and most likely displaces the αC-helix to an 'OUT' position that leads to an inactive conformation.

Inhibiting the Catalytic Activity of CRAF within the BRAF^{D594G}:CRAF- The two FDA approved BRAF drugs, dabrafenib and vemurafenib, have a positive clinical outcome for patients harboring oncogenic BRAF^{V600E}, but are less effective towards non-V600 BRAF mutants.(4,9) Other labs have suggested that targeting MEK or EGFR is a viable treatment option for class 3 BRAF tumors,(8) but currently no RAF directed therapies are available. There are three types of BRAF inhibitors which are grouped by how they orient the αC-helix or DFG motif.(4) Type I inhibitors, such as SB-590885 (SB), lock BRAF into an active conformation with αC-helix-IN and DFG-IN. Type I$^{1/2}$ inhibitors, including Dabrafenib (dab), Vemurafenib (vem), PLX-4720 (PLX), and PB-PLX7904 (PB), orient the αC-helix-OUT and DFG-IN conformation. Type II inhibitors, such as AZ-628 (AZ), adopt the αC-helix-IN and DFG-OUT conformation. The αC-helix-IN (type I/II) configuration allows for inhibitor binding to both protomers of BRAF with equal potency; however, type I$^{1/2}$ inhibitors lock the αC-helix-OUT configuration to sterically hinder occupancy for the second protomer which leads to negative cooperativity. Although each category of inhibitor is effective at inhibiting BRAF^{V600E}, (17) they have very different binding mechanisms that regulate

dimeric WT BRAF differently. WT BRAF displays drug resistance and paradoxical activation towards Type I$^{1/2}$ inhibitors.

Here we evaluate the different categories of RAF inhibitors against BRAF^{D594G}:CRAF heterodimers. Differential scanning fluorimetry (DSF) results show that all the tested ATP-competitive inhibitors bind to CD-BRAF^{D594G} (Figure 5A), although BRAF^{D594G} could not bind to ATP (Figure S1). However, it remains unclear whether these inhibitors can trigger paradoxical activation in cells expressing BRAF^{D594G}. Additionally, our MD simulations have shown that the D594G:CRAF heterodimer is in a different conformation than the CRAF homodimer, therefore different drug response is expected between RAF homo- and heterodimers. To address these concerns, we applied cell-based assays to evaluate the potency of the selected inhibitors in HEK293 cells transiently transfected with BRAF^{D594G} and CRAF. BRAF^{V600E} and WT BRAF/CRAF were used as the controls (Figure 5B&C).

Pan-RAF inhibitors, such as AZ, are active against ARAF, BRAF, and CRAF with equal potency, thus titrating different concentrations of AZ showed inhibition at 0.1 μM (Figure 5D). The potency of AZ towards BRAF^{D594G}:CRAF isn't surprising, because this inhibitor has been shown to have low nanomolar potency towards CRAF in cell-free experiments.(23) Additionally, Noeparast *et al.* show a similar inhibition profile towards the D594G:CRAF heterodimer.(24) PB is a paradox-breaking inhibitor designed to minimize paradoxical activation,(25) but type I$^{1/2}$ inhibitors have much lower activity towards dimeric RAF, and no significant activity of PB towards the BRAF^{D594G}:CRAF heterodimer was observed (Figure 5E). Although AZ and SB target monomeric and dimeric BRAF with similar potency, SB only shows inhibition at the highest concentration tested toward BRAF^{D594G}:CRAF (Figure 5D&F), most likely due to its low potency towards CRAF. We also tested PLX-4720 (PLX) that is known to potently inhibit monomeric BRAF, and it only shows slight inhibition of the BRAF^{D594G}:CRAF heterodimer at the highest concentration of drug used (Figure 5G). AZ, a representative of type II pan-RAF inhibitors, exhibit inhibition of the BRAF^{D594G}:CRAF heterodimer at the lowest concentrations tested. Additionally, Karoulia *et al.* have identified that pan-RAF inhibitors have a slower off rate and dissociate the RAF/MEK complex.(4) These data support that pan-RAF inhibitors might be a good scaffold for rationally designed BRAF^{D594G}:CRAF inhibitors.

Notably, none of the ATP-competitive inhibitors induced paradoxical activation even though binding of DFG-IN inhibitors: Dab, PLX, and SB show slight enhancement of BRAF^{D594G}:CRAF heterodimerization (Figure 5H). In contrary, WT BRAF:CRAF heterodimers were paradoxically activated by dabrafenib under the same conditions (Figure 5C).(24) Due to the correlation of BRAF^{D594G} and P-loop autoinhibitory phosphorylation, we introduced Ser465A/Ser467A (SS/AA) mutation to WT BRAF to prevent P-loop phosphorylation. No paradoxical activation was observed for BRAF$^{SS/AA}$, suggesting that P-loop phosphorylation plays a role in paradoxical activation (Figure 5I). Under this scenario, kinase-dead BRAF abolishes P-loop phosphorylation of catalytically active CRAF within the BRAF^{D594G}:CRAF dimer, which also evades paradoxical activation. This model is consistent with Holderfield *et al.* in which they highlighted that ATP-competitive inhibitor relieves inhibitory P-loop phosphorylation of WT RAF to trigger paradoxical activation.(26) Another possibility is that the BRAF^{D594G} mutation already makes BRAF a perfect allosteric activator and inhibitor binding makes no further enhancement regarding its ability to transactivate CRAF. (Figure 5J).

We also treated melanoma cells (WM3629) that are expressing BRAF^{D594G} and NRAS^{G12D} with AZ (Figure 5K). The pan-RAF inhibitor completely abolished MEK/ERK signaling at 1 μM, which supports that AZ can inhibit the MAPK pathway in a short time period. However, long exposure of 96 h still exhibited ~ 50% of cell growth at the highest concentration (5 μM) of drug treated (Figure 5L), suggesting that BRAF^{D594G}:CRAF heterodimers display drug resistance towards ATP-competitive inhibitors. This is consistent with another group who showed that AZ alone cannot fully eliminate growth of cells harboring various RAS mutations.(27) The discrepancy between the amount of drug required for MAPK inhibition and cancer cell death highlight that pan-RAF inhibitors

might not be a viable therapeutic treatment for class 3 BRAF mutations.

RAF Dimer Breaker is Active Against BRAF^{D594G}:CRAF- Recognizing dimerization of BRAF^{D594G} and CRAF is critical for both protein stability and kinase activity poises the dimer interface as a promising drug target. Previously, we developed a 10-mer peptide (Braftide) that shows efficient inhibition and degradation of WT BRAF and BRAF^{G469A} both *in vitro* and in a variety of cells exhibiting either RAS dependence or independence, respectively.(28) To extend the same study to BRAF^{D594G}:CRAF heterodimers, we titrated 0-100 μM of TAT-Braftide into HEK293 cells overexpressing the BRAF^{D594G}:CRAF heterodimers (Figure 6A). This peptide inhibitor not only shows inhibition of MAPK signaling, but also degradation of the BRAF^{D594G}:CRAF heterodimer at as low as 25 μM. We applied a similar experiment to WM3629 cancer cells (Figure 6B). TAT-Braftide exhibits degradation of BRAF^{D594G} and CRAF at concentrations as low as 2.5 μM in WM3629 cells. We treated WM3629 cells with TAT-Braftide for 48 h to observe the activity of this peptide by cell viability assays, which showed dose-dependent inhibition of cell growth and an EC_{50} of 11.05 ± 1.12 μM (Figure 6C). Together, these results highlight that BRAF^{D594G}:CRAF heterodimers are still sensitive to dimer breakers, despite the fact that it has a stronger dimer interface than BRAF homodimers.

Conclusions

In our study, we focused on BRAF^{D594G}, a representative of kinase-dead BRAF mutants to better understand the non-catalytic function of BRAF. Interestingly, protein kinases have evolved to have allosteric scaffolding properties, in addition to their inherent capability of catalyzing the transfer of the γ-phosphate from ATP to tyrosine, serine, or threonine residues in the substrate proteins. Pseudokinases are an example of enzymes that have diverged to primarily function as scaffolds, such as kinase-impaired HER3 which allosterically activate other EGFR/HER family members through asymmetric dimerization.(29) Another example is kinase-suppressor of RAS (KSR) which has been shown to function as a scaffolding protein to allosterically regulate RAF and MEK.(30) BRAF kinase has both scaffold function and catalytic activity that are integrated to determine the final output of RAF signaling. Intriguingly, ATP-competitive inhibitors can differentially alter the two functions to trigger paradoxical activation, in which the scaffold function of BRAF is exaggerated to compensate the inhibited kinase activity, and the overall outcome is enhanced RAF signaling. However, it is hard to pinpoint which role is more significant than the other. The kinase-dead BRAF mutant provides a valuable tool to elucidate the allosteric consequence of mutations that are linked to cancer.

Our biophysical experiments and MD simulations show that BRAF^{D594G} is more prone to dimerization than BRAF^{WT} due to the positioning of the αC-helix towards the IN conformation. In addition, the activation loop of BRAF^{D594G} is beginning to unwind from the AS-H1 loop towards full extension, which is a prerequisite for kinase activation. The extended activation loop stabilizes the regulatory spine (R-spine) and αC-helix into a conformation suitable for dimerization,(30) thus BRAF^{D594G} is in a partially active, dimerization-competent conformation leading to enhanced allosteric function. Interestingly, the most recent cryo-EM structure of BRAF in complex with ATP analog ATP-γS suggests that ATP binding is critical to maintain the autoinhibited state. (22) Since BRAF^{D594G} can't bind ATP, this feature further stabilizes the active conformation of BRAF to support RAF dimerization.

Experiments with other pseudokinases: VRK, MLKL, STRAD, ERBB3, and JAK2, have emphasized that ATP binding can enhance allosteric activation of the associated partner for some pseudokinases.(31-34) However, BRAF^{D594G} does not bind ATP but still functions as an allosteric activator. In addition, the A481F or A373F mutations, that interfere with ATP binding to BRAF or CRAF respectively, have been shown to constitutively dimerize with and activate the RAF binding partner.(35) These results combined with ours suggests that the alignment of the catalytic spine (C-spine) is not necessary for the scaffold function of BRAF.

Enhanced signaling required to drive MAPK pathway activation in cells is attained by either increased enzyme activity or reduced negative regulatory feedback effects.(36) We show that BRAF^{D594G}:CRAF heterodimers are more active than CRAF alone and have an activity that is

comparable to that of the BRAF:CRAF heterodimer. This increase in activity could be attributed to BRAF^{D594G}:CRAF heterodimers bypassing inhibitory P-loop autophosphorylation that negatively controls WT RAF activity in cells.(17) The glycine rich P-loop (Gly-X-Gly-X-X-Gly motif) is highly conserved among protein kinases and is known to position the α-/β-phosphates of ATP for optimal γ-phosphoryl transfer during catalysis. In addition, it is believed that the hydrophobic interactions between P-loop and activation loop stabilizes the inactive configuration of the kinase.(37) Protein kinases share a universal activation mechanism, in which conformational changes in three conserved structural motifs at the active site: the activation loop, the DFG motif, and the αC-helix, determine the transition from the inactive to the active conformation.(38) The effect of P-loop phosphorylation has not been well studied. Our MD simulation results demonstrate that phosphorylated P-loop disfavors the side-to-side dimer configuration, which in turn supports the non-productive position of the αC-helix. Here we have confirmed the existence of a crosstalk among P-loop and the three motifs that modulates the conformational equilibrium of the BRAF kinase. These data unveil P-loop as an important structural feature involved in positioning the αC-helix, depending on its phosphorylation status. Given that the Ser465/Ser467 residues are highly conserved among P-loop (Supplementary Figure S4A&B), it is appealing to propose a similar role for the conserved Ser/Thr residues in other kinase families.

In the past decades, the molecular mechanism of RAF regulation was mostly derived from structures of isolated kinase domains or fragments of other domains. The cryo-EM structures of full-length BRAF-MEK1-14-3-3 complexes were solved recently, (22) providing a more comprehensive structural characterization of RAF. In those structures, both autoinhibited and fully activated BRAF were captured, demonstrating that MEK1 and 14-3-3 are both involved in stabilizing BRAF in the active or inactive conformations. (22) Our findings introduce an additional layer of complexity to the precise mechanism of BRAF activation. Our lab previously identified that the presence of MEK1 decreases overall BRAF autophosphorylation while increases phosphorylation of the activation loop *in vitro*, suggesting a new allosteric role of MEK1, other than functioning as a substrate of RAF kinases. (15) In light of those, we propose one model for RAF regulation under physiological conditions, as shown in Figure 7. After RAS-initiated RAF dimerization, MEK binding primes the activation loop of RAF for trans-phosphorylation,(15) which leads to maximal RAF activation and subsequent MEK phosphorylation. Upon dissociation of phosphorylated MEK, RAF trans-phosphorylates the P-loop to diminish its own kinase activity. Meanwhile, this negative regulation loop can be dampened by protein phosphatases to maintain highest RAF activity. In this model, P-loop autophosphorylation is a self-sustained mechanism to self-limit its kinase activity *in vivo*.

Two main models have emerged to shed light on the molecular mechanism of paradoxical activation. The first model suggests that binding of RAF inhibitors increases dimerization of drug-bound RAF with inhibitor-free RAF, which results in RAS-dependent MEK/ERK activation.(5) Similarly, Heidorn *et al.* have related this model to how kinase-dead BRAF activates CRAF in a RAS-dependent manner.(12) The second model identifies that RAF inhibitors activate MEK/ERK by relieving inhibitory RAF autophosphorylation.(26) In our work, we provide evidence reconciling the two models of paradoxical activation. We show that inhibitory autophosphorylation occurs in *trans*, not *cis*, thus oncogenic BRAF^{D594G} can evade this negative feedback loop by eliminating autophosphorylation of CRAF in the BRAF^{D594G}:CRAF heterodimer due to the lack of enzyme activity. RAF ATP-competitive inhibitors don't display paradoxical activation in the context of BRAF^{D594G}:CRAF heterodimer, providing direct evidence that relief of p-loop phosphorylation by RAF inhibitors is capable of activating MAPK signaling. Additionally, BRAF^{D594G} and CRAF readily form a stable dimer, hence RAF inhibitors could no longer boost the allosteric function of BRAF.

The increased frequency of non-V600 mutations detected in lung and other cancers highlights the urgency of targeting class 3 BRAF.(39) Although there have been several proposed strategies to combat dimer-dependent BRAF mutations, such as targeting CRAF, MEK, and EGFR;(3,9,24) there are currently no clinically approved drugs that are

designed specifically to treat tumors harboring class 3 BRAF mutations. Since the approval of targeting BRAF^{V600E} mutations with vemurafenib or dabrafenib in combination with MEK inhibitors, this has been a suggested strategy to treat other BRAF mutations. Combination therapy with RAF and MEK inhibitors in cell lines harboring class 3 BRAF mutations have been previously analyzed.(8,24) In these experiments, they show that MEK inhibitors alone or in combination with RAF inhibitors decrease MAPK pathway activation and induce cellular apoptosis. Although treatment with MEK inhibitors is promising, cytotoxicity is an inevitable concern, thus more specific inhibitors are urgently needed. Our results on inhibiting phosphorylation of S729 of BRAF make the C-terminal 14-3-3 binding site a druggable target for class 3 BRAF mutations. Similarly, Kondo *et al.* identified that targeting the αI-helix, at the 14-3-3 binding interface, could have improved therapeutic efficacy in dimer-dependent BRAF mutations.(40)

Braftide activity towards BRAF^{D594G}:CRAF heterodimers in cells suggests that allosteric inhibitors targeting the dimer interface could have an improved therapeutic index. In addition, we show that pan-RAF ATP-competitive inhibitors show initial inhibition of BRAF^{D594G}:CRAF heterodimer activity, but prolonged exposure fails to abolish WM3629 cancer cell growth. Moreover, Montagut *et al.* suggest that overexpression of CRAF, as we see with the co-transfection of BRAF^{D594G}:CRAF, can lead to acquired resistance to pan-RAF inhibitors,(41) suggesting that targeting the ATP binding pocket of CRAF alone might not be the best therapeutic strategy. Hence, rationally designed drugs with improved selectivity are required to target CRAF or the dimer interface for class 3 BRAF mutations.

Altogether our work complements the current understanding of kinase-impaired/kinase-dead BRAF mutations, while highlighting key biochemical properties of the most common kinase-dead mutation, BRAF^{D594G}. These results identify how BRAF^{D594G}:CRAF heterodimers sustain increased MEK/ERK activation in cancer cells, while exposing a new allosteric site, at the dimer interface, to target class 3 BRAF mutations.

Experimental Section:

Compounds and Reagents Dabrafenib, AZ-628, PLX-4720, PB-PLX7904, SB-590885, and Dorsomorphin (Compound C) 2HCl were purchased from Selleckchem. 10 mM inhibitor stocks were made in DMSO (RAF inhibitors)/double-distilled water (AMPKi) and stored at -20°C. ATP γ-P32 (#NEG002Z250UC) was purchased from Perkin Elmer. Polyethylenimine Hydrochloride-MAX (PEI Max) was purchased from Polysciences (#24765). Fetal Bovine Serum (FBS) was purchased from Gemini Bio-Products (#100-602). L-glutamine (#25030-081), Dulbecco's Modified Eagle Medium (DMEM #11995-065), Trypsin-EDTA (#25300-054), OptiMEM (31985-070), PBS (10010-023) were purchased from Gibco. Sypro-orange dye (#S6651) was purchased from Invitrogen. Braftide was synthesized as previously described.(28) All other reagents were purchased without further purification.

Antibodies Anti-FLAG M2 mouse (#F1804), anti-FLAG M2 rabbit (#F2555), anti-FLAG M2 magnetic resin (#M8823), pCRAF (pSer338) antibody (#05-538) were purchased from Sigma Aldrich. HA antibody (#26183) was purchased from Invitrogen. Profinity IMAC Ni charged resin (#156-0131) was purchased from Bio-Rad. Anti-p-MEK1/2 Ser217/221 (#9154), anti-pERK1/2 (#4370), anti-BRAF (#14814), anti-CRAF (#9422), Raptor (#2280), and phospho-Raptor (#89146) were purchased from Cell Signaling. Actin antibody was purchased from Sigma (#A2228). Phospho-BRAF (pSer729) antibody (ab124794) was purchased from Abcam.

Plasmids *wild-type* BRAF/6x-HIS/FLAG and CRAF/6x-HIS/HA were designed as previously described.(15) BRAF-D594G/6x-HIS/FLAG, BRAF-D594GΔN-tail/FLAG, BRAF-D594GΔRBD/FLAG, BRAF-D594GΔCR2/FLAG, and BRAF-D594GΔSSDD/FLAG, BRAF-S465D/S467D/6x-HIS/FLAG, and CRAF/FLAG/MBP were created using common cloning procedures with pCDNA^{TM} 4/TO (Invitrogen) as the vector. Wild-type CD-BRAF 16 mutations was a gift from Dr. Ronen Marmorstein's lab,(42) and wild-type CD-BRAF (aa. 442-723), with the SSDD motif added, was inserted into pET-21(+) vector (Sigma-Aldrich). CD-D594G/6x-HIS was generated using common cloning procedures with pET21+ (Sigma-Aldrich) as the vector.

Cell lines WM3629 and HTB177 were purchased from Rockland and HTCC, respectively. HEK293 cells were a gift from Dr. Catherine Moore (USciences).

CD-BRAF Purification CD-BRAF-6xHIS was transformed into BL21 codon plus *E. coli* cells and grown at 37°C to an optical density 600 nm (OD600) of 0.6-0.8 then 1 mM IPTG and incubated at 16°C for overnight incubation with stirring at 200 rpm. The harvested pellet was resuspended in lysis buffer (50 mM HEPES buffer pH 7.4, 250 mM NaCl, 50 mM KCl, 10 mM Imidazole, 10 mM β-ME, 10% Glycerol, and protease inhibitor tablet (Sigma cat#11836170001)) then lysed with a sonicator. The lysed suspension was centrifuged to separate the clarified supernatant, then the supernatant was applied to pre-equilibrated Nickel resin and incubated with rotation at 4°C for 1-2 h. After resin incubation, the supernantant/resin slurry was added to a gravity column and washed with wash buffer (50 mM HEPES pH 7.4, 250 mM NaCl, 10 mM imidazole, and 10% glycerol). 50-250 mM of Imidazole was spiked into low salt buffer (50 mM HEPES pH 7.4, 250 mM NaCl, and 10% glycerol) to elute the protein, which was pooled and concentrated, using a millipore concentrator (cat# UFC803024), before injecting onto size-exclusion chromatography (column: Superdex 200 10/300 GL cat # 28-9909-44). The corresponding peaks were analyzed with SDS-PAGE, then pooled, concentrated, and aliquotted. These aliquots were flash frozen in liquid nitrogen and stored at -80°C.

Analytical Ultracentrifugation The Velocity AUC experiment was performed as previously described.(42) Briefly, 10-15 μM of wild-type CD-BRAF and CD-D594G were centrifuged at 42,000 r.p.m. for ~ 8 h while data was collected over the entire time frame. The results were analyzed with SEDFIT to calculate the continuous c(S) distribution and data was graphed using Origin.

Molecular Dynamics Simulations The molecular dynamics simulations were performed as previously described.(17) In brief, the crystal structures that were acquired from the respective PDB file were cleaned up and solvated in a periodic box using TIP3P water molecules. The ff14SB(43) force field was used on the proteins. GPUimplemented Amber18 was utilized for each MD simulation.(44) All systems were equilibrated using the same protocol for solvent minimization, heating, and NPT simulation at 1 atm and 300K. Production runs using the NVT system at 300K were then applied for 200 to 400 ns per system. The trajectories were then investigated with the cpptraj program in the Amber18 package for hydrogen bond interactions, distance, RMSD, etc. as conveyed in the text.

Transient Transfection into Mammalian Cells HEK293 cells were transiently transfected as previously described.(17) In Brief, 0.5-1 million HEK293 cells were plated onto 12- or 6-well plates respectively then were incubated overnight until the cells reached a 40-60% confluency. DNA (0.5-2 μg) was mixed with PEI-MAX in a 1:3 ratio. DNA:PEI-MAX was added to fresh DMEM on the HEK293 cells. The cells were washed with ice-cold PBS after 24-48 h then lysed in 4% SDS. The harvested lysate was applied to homogenizer columns and the flow-through protein concentration was analyzed using a BCA kit (Pierce cat #23225). 10-40 μg of lysates were used for Western Blot analyses.

BRAF:CRAF Co-immunoprecipitation For immunoprecipitation, 5 million HEK293 cells were plated onto a 10 cm dish and incubated overnight at 37°C with 5% CO_2. Once the cells reached a confluency of 40-60%, the DMEM media was aspirated out and fresh DMEM was added. A total of 10 μg of DNA (5 μg + 5 μg for Co-transfections) was mixed with 30 μg of PEI-MAX for 25 minutes then added to the plated cells for 48 h at 37°C with 5 % CO_2. For inhibitor treatment, the cells were washed with PBS then DMEM containing DMSO (0.5% final) or inhibitor was added to the cells and incubated for 1 hr at 37°C with 5 % CO_2. Cells were washed again with ice-cold PBS then lysed in 1 mL of lysis buffer (50 mM HEPES pH 7.4, 150 mM NaCl, 0.1% NP40 (IGEPAL630), 1 mM EDTA, 5% glycerol, 1 mM PMSF, 20 mM βGP, 2.5 mM sodium pyrophosphate, and protease inhibitor) for 2 h with rotation at 4°C. The lysate was clarified and 0.5-1 mg of lysate was applied to 10 μL of pre-equilibrated Amylose or FLAG resin for 2 h with rotation at 4°C. The resin was washed 5x (5 minutes each wash) with lysis buffer, then resuspended in 2x dilution buffer (25 mM HEPES pH 7.4, 0.125 mg/mL BSA, and 300 mM NaCl) for kinase assays

or quenched with 4x loading dye to be analyzed by Western blotting.

Kinase-Dead MEK1-K97M Purification Kinase-dead MEK1-K97M/6xHIS/GST protein was purified from BL21 codon plus *E. coli* as previously described.(15) Briefly, the cells expressing MEK1 were harvested then lysed in lysis buffer (20 mM HEPES pH 7.4, 150 mM NaCl, 10 mM βME, Sigma Aldrich Complete^{TM} EDTA-Free protease inhibitor tablets (product # 11836170001), 5 mM Imidazole, and 5% Glycerol) with sonication (1 mg/mL of lysozyme was used to help with lysis). The supernatant was added to equilibrated Nickel resin and incubated for 2 hours. The protein bound resin was washed with low salt buffer (20 mM HEPES, 150 mM NaCl, and 5 % glycerol). MEK1 was eluted with elution buffer (150 mM imidazole, 20 mM HEPES, 150 mM NaCl, and 5 % glycerol) and further purified, concentrated to >0.1 mg/mL and stored as described above.

Western Blotting-Based Kinase Assay The kinase assay was performed as previously described.(17) In brief, the purified proteins or Co-IP products were diluted with 2x dilution buffer and combined with 2x cocktail buffer (25 mM HEPES pH 7.4, 20 mM $MgCl_2$, 1 mM DTT, 50 mM β-glycerolphosphate, 0.2-2 μM MEK (0.1-1 μM final), and 2000 μM ATP) for 5-10 min, unless another time is indicated at 30°C. The reaction was quenched using 4x loading dye then analyzed by SDS-PAGE immunoblotting. The nitrocellulose membranes were probed with the suitable primary and secondary antibodies and imaged using fluorescence based approaches on a GE Typhoon imager. Analyses of the immunoblots were analyzed using ImageJ software.

In-Gel Radioactive Assay As described previously,(17) purified or CoIP proteins were mixed with a 2x cocktail buffer (25 mM HEPES pH 7.4, 20 mM $MgCl_2$, 50 mM β- glycerolphosphate, 1mM DTT, 4 mM Na_3VO_4, 200 uM ATP, and 1 uCi radioactive ATP). A final concentration of 1.3 μM MEK was spiked into the cocktail buffer for tests that contained MEK and ATP. The reaction was incubated at 30 minutes at RT before being transferred to SDS-Page, dried, and imaged on a Typhoon imager.

Differential Scanning Fluorimetry CD-D594G aliquots were diluted in DSF buffer (25 mM HEPES pH 7.0, 150 mM NaCl) to a concentration of 5 μM (final). To a 384-well PCR plate (Thermo Scientific cat # AB-1384), 15 μL of CD-D594G, 4 μL of SyproOrange (5x final), and 1 μL of inhibitor in DMSO (25 μM final) were added. The plate was sealed with adhesive seal sheets (Thermo Scientific cat# AB-1170) then spun down and heated from 20-95°C on QuantStudio 7 Flex (Applied Biosystems) with a ramp rate of 0.015°C/s. The protein melt curves were produced and the first derivative of the curve was used to analyze the data. The data was examined and plotted using Origin.

Cell Viability The cell viability assay was performed as previously described.(28) In brief, WM3629 cells were plated onto a 96-well plate for 24 hours before treatment. TAT-Braftide or AZ-628 were titrated on to the cells at the indicated concentrations for 48 or 96 h, respectively. The drug media was switched out every 24 h, then the WST reagent was added, in a 1:10 ratio, and incubated for 4 h at 37°C. Absorbance readings were measured for the plate at 450 nm.

Accession codes:

BRAF: Uniprot ID# P15056

CRAF: Uniprot ID# P04049

MEK1: Uniprot ID# Q02750

Acknowledgements: The study was funded by the W.W. Smith Charitable Fund and NIGMS (1R15GM128099-01) to Z. Wang and the Spiers Fellowship to N. Cope and A. Gunderwala. Special thanks to the Marmostein Lab at the Perelman School of Medicine for help with biophysical experiments and for useful discussions.

Conflict of Interest: The authors declare that they have no conflicts of interest with the contents of this article.

The content is solely the responsibility of the authors and does not necessarily represent the official views of the National Institutes of Health

References

1. Lavoie, H., and Therrien, M. (2015) Regulation of RAF protein kinases in ERK signalling. *Nature Reviews Molecular Cell Biology* **16**, 281-298
2. Davies, H., Bignell, G. R., Cox, C., Stephens, P., Edkins, S., Clegg, S., Teague, J., Woffendin, H., Garnett, M. J., Bottomley, W., Davis, N., Dicks, E., Ewing, R., Floyd, Y., Gray, K., Hall, S., Hawes, R., Hughes, J., Kosmidou, V., Menzies, A., Mould, C., Parker, A., Stevens, C., Watt, S., Hooper, S., Wilson, R., Jayatilake, H., Gusterson, B. A., Cooper, C., Shipley, J., Hargrave, D., Pritchard-Jones, K., Maitland, N., Chenevix-Trench, G., Riggins, G. J., Bigner, D. D., Palmieri, G., Cossu, A., Flanagan, A., Nicholson, A., Ho, J. W. C., Leung, S. Y., Yuen, S. T., Weber, B. L., Seigler, H. F., Darrow, T. L., Paterson, H., Marais, R., Marshall, C. J., Wooster, R., Stratton, M. R., and Futreal, P. A. (2002) Mutations of the BRAF gene in human cancer. *Nature* **417**, 949-954
3. Yao, Z., Torres, N. M., Tao, A., Gao, Y., Luo, L., Li, Q., de Stanchina, E., Abdel-Wahab, O., Solit, D. B., Poulikakos, P. I., and Rosen, N. (2015) BRAF Mutants Evade ERK-Dependent Feedback by Different Mechanisms that Determine Their Sensitivity to Pharmacologic Inhibition. *Cancer Cell* **28**, 370-383
4. Karoulia, Z., Wu, Y., Ahmed, Tamer A., Xin, Q., Bollard, J., Krepler, C., Wu, X., Zhang, C., Bollag, G., Herlyn, M., Fagin, James A., Lujambio, A., Gavathiotis, E., and Poulikakos, Poulikos I. (2016) An Integrated Model of RAF Inhibitor Action Predicts Inhibitor Activity against Oncogenic BRAF Signaling. *Cancer Cell* **30**, 485-498
5. Poulikakos, P. I., Zhang, C., Bollag, G., Shokat, K. M., and Rosen, N. (2010) RAF inhibitors transactivate RAF dimers and ERK signalling in cells with wild-type BRAF. *Nature* **464**, 427-430
6. Hatzivassiliou, G., Song, K., Yen, I., Brandhuber, B. J., Anderson, D. J., Alvarado, R., Ludlam, M. J. C., Stokoe, D., Gloor, S. L., Vigers, G., Morales, T., Aliagas, I., Liu, B., Sideris, S., Hoeflich, K. P., Jaiswal, B. S., Seshagiri, S., Koeppen, H., Belvin, M., Friedman, L. S., and Malek, S. (2010) RAF inhibitors prime wild-type RAF to activate the MAPK pathway and enhance growth. *Nature* **464**, 431-435
7. Chang, M. T., Asthana, S., Gao, S. P., Lee, B. H., Chapman, J. S., Kandoth, C., Gao, J., Socci, N. D., Solit, D. B., Olshen, A. B., Schultz, N., and Taylor, B. S. (2016) Identifying recurrent mutations in cancer reveals widespread lineage diversity and mutational specificity. *Nature biotechnology* **34**, 155-163
8. Yao, Z., Yaeger, R., Rodrik-Outmezguine, V. S., Tao, A., Torres, N. M., Chang, M. T., Drosten, M., Zhao, H., Cecchi, F., Hembrough, T., Michels, J., Baumert, H., Miles, L., Campbell, N. M., de Stanchina, E., Solit, D. B., Barbacid, M., Taylor, B. S., and Rosen, N. (2017) Tumours with class 3 BRAF mutants are sensitive to the inhibition of activated RAS. *Nature* **548**, 234-238
9. Nieto, P., Ambrogio, C., Esteban-Burgos, L., Gomez-Lopez, G., Blasco, M. T., Yao, Z., Marais, R., Rosen, N., Chiarle, R., Pisano, D. G., Barbacid, M., and Santamaria, D. (2017) A Braf kinase-inactive mutant induces lung adenocarcinoma. *Nature* **548**, 239-243
10. Joseph, E. W., Pratilas, C. A., Poulikakos, P. I., Tadi, M., Wang, W., Taylor, B. S., Halilovic, E., Persaud, Y., Xing, F., Viale, A., Tsai, J., Chapman, P. B., Bollag, G., Solit,

D. B., and Rosen, N. (2010) The RAF inhibitor PLX4032 inhibits ERK signaling and tumor cell proliferation in a V600E BRAF-selective manner. *Proceedings of the National Academy of Sciences* **107**, 14903-14908

11. Rajakulendran, T., Sahmi, M., Lefrancois, M., Sicheri, F., and Therrien, M. (2009) A dimerization-dependent mechanism drives RAF catalytic activation. *Nature* **461**, 542-545
12. Heidorn, S. J., Milagre, C., Whittaker, S., Nourry, A., Niculescu-Duvas, I., Dhomen, N., Hussain, J., Reis-Filho, J. S., Springer, C. J., Pritchard, C., and Marais, R. (2010) Kinase-Dead BRAF and Oncogenic RAS Cooperate to Drive Tumor Progression through CRAF. *Cell* **140**, 209-221
13. Grasso, M., Estrada, M. A., Berrios, K. N., Winkler, J. D., and Marmorstein, R. (2018) N-(7-Cyano-6-(4-fluoro-3-(2-(3-(trifluoromethyl)phenyl)acetamido)phenoxy)benzo[d] thiazol-2-yl)cyclopropanecarboxamide (TAK632) Promotes Inhibition of BRAF through the Induction of Inhibited Dimers. *J Med Chem* **61**, 5034-5046
14. Thevakumaran, N., Lavoie, H., Critton, D. A., Tebben, A., Marinier, A., Sicheri, F., and Therrien, M. (2015) Crystal structure of a BRAF kinase domain monomer explains basis for allosteric regulation. *Nat Struct Mol Biol* **22**, 37-43
15. Cope, N., Candelora, C., Wong, K., Kumar, S., Nan, H., Grasso, M., Novak, B., Li, Y., Marmorstein, R., and Wang, Z. (2018) Mechanism of BRAF Activation through Biochemical Characterization of the Recombinant Full-Length Protein. *Chembiochem : a European journal of chemical biology* **19**, 1988-1997
16. Qin, J., Xie, P., Ventocilla, C., Zhou, G., Vultur, A., Chen, Q., Liu, Q., Herlyn, M., Winkler, J., and Marmorstein, R. (2012) Identification of a novel family of BRAF(V600E) inhibitors. *J Med Chem* **55**, 5220-5230
17. Cope, N., Novak, B., Candelora, C., Wong, K., Cavallo, M., Gunderwala, A., Liu, Z., Li, Y., and Wang, Z. (2019) Biochemical Characterization of Intact Oncogenic BRAFV600E Together With Molecular Dynamics Simulations Provide Insight into the Activation and Inhibition Mechanisms of RAF Kinases. *Chembiochem : a European journal of chemical biology* **20**, 2850-2861
18. Weber, C. K., Slupsky, J. R., Kalmes, H. A., and Rapp, U. R. (2001) Active Ras induces heterodimerization of cRaf and BRaf. *Cancer Res* **61**, 3595-3598
19. Chen, S. H., Zhang, Y., Van Horn, R. D., Yin, T., Buchanan, S., Yadav, V., Mochalkin, I., Wong, S. S., Yue, Y. G., Huber, L., Conti, I., Henry, J. R., Starling, J. J., Plowman, G. D., and Peng, S. B. (2016) Oncogenic BRAF Deletions That Function as Homodimers and Are Sensitive to Inhibition by RAF Dimer Inhibitor LY3009120. *Cancer Discov* **6**, 300-315
20. Freeman, A. K., Ritt, D. A., and Morrison, D. K. (2013) The importance of Raf dimerization in cell signaling. *Small GTPases* **4**, 180-185
21. Yuan, J., Ng, W. H., Yap, J., Chia, B., Huang, X., Wang, M., and Hu, J. (2018) The AMPK inhibitor overcomes the paradoxical effect of RAF inhibitors through blocking phospho-Ser-621 in the C terminus of CRAF. *The Journal of biological chemistry* **293**, 14276-14284
22. Park, E., Rawson, S., Li, K., Kim, B. W., Ficarro, S. B., Pino, G. G., Sharif, H., Marto, J. A., Jeon, H., and Eck, M. J. (2019) Architecture of autoinhibited and active BRAF-MEK1-14-3-3 complexes. *Nature* **575**, 545-550
23. Khazak, V., Astsaturov, I., Serebriiskii, I. G., and Golemis, E. A. (2007) Selective Raf Inhibition in Cancer Therapy. *Expert opinion on therapeutic targets* **11**, 1587-1609

24. Noeparast, A., Giron, P., De Brakeleer, S., Eggermont, C., De Ridder, U., Teugels, E., and De Greve, J. (2018) Type II RAF inhibitor causes superior ERK pathway suppression compared to type I RAF inhibitor in cells expressing different BRAF mutant types recurrently found in lung cancer. *Oncotarget* **9**, 16110-16123
25. Zhang, C., Spevak, W., Zhang, Y., Burton, E. A., Ma, Y., Habets, G., Zhang, J., Lin, J., Ewing, T., Matusow, B., Tsang, G., Marimuthu, A., Cho, H., Wu, G., Wang, W., Fong, D., Nguyen, H., Shi, S., Womack, P., Nespi, M., Shellooe, R., Carias, H., Powell, B., Light, E., Sanftner, L., Walters, J., Tsai, J., West, B. L., Visor, G., Rezaei, H., Lin, P. S., Nolop, K., Ibrahim, P. N., Hirth, P., and Bollag, G. (2015) RAF inhibitors that evade paradoxical MAPK pathway activation. *Nature* **526**, 583-586
26. Holderfield, M., Merritt, H., Chan, J., Wallroth, M., Tandeske, L., Zhai, H., Tellew, J., Hardy, S., Hekmat-Nejad, M., Stuart, Darrin D., McCormick, F., and Nagel, Tobi E. (2013) RAF Inhibitors Activate the MAPK Pathway by Relieving Inhibitory Autophosphorylation. *Cancer Cell* **23**, 594-602
27. Wang, Z., Yin, M., Chu, P., and Lou, M. (2019) STAT3 inhibitor sensitized KRAS-mutant lung cancers to RAF inhibitor by activating MEK/ERK signaling pathway. *Aging* **11**, 7187–7196
28. Gunderwala, A. Y., Nimbvikar, A. A., Cope, N. J., Li, Z., and Wang, Z. (2019) Development of Allosteric BRAF Peptide Inhibitors Targeting the Dimer Interface of BRAF. *ACS Chem Biol* **14**, 1471-1480
29. Jura, N., Shan, Y., Cao, X., Shaw, D. E., and Kuriyan, J. (2009) Structural analysis of the catalytically inactive kinase domain of the human EGF receptor 3. *Proceedings of the National Academy of Sciences of the United States of America* **106**, 21608-21613
30. Hu, J., Stites, Edward C., Yu, H., Germino, Elizabeth A., Meharena, Hiruy S., Stork, Philip J. S., Kornev, Alexandr P., Taylor, Susan S., and Shaw, Andrey S. (2013) Allosteric Activation of Functionally Asymmetric RAF Kinase Dimers. *Cell* **154**, 1036-1046
31. Shaw, A. S., Kornev, A. P., Hu, J., Ahuja, L. G., and Taylor, S. S. (2014) Kinases and Pseudokinases: Lessons from RAF. *Molecular and Cellular Biology* **34**, 1538-1546
32. Zeqiraj, E., Filippi, B. M., Goldie, S., Navratilova, I., Boudeau, J., Deak, M., Alessi, D. R., and van Aalten, D. M. (2009) ATP and MO25alpha regulate the conformational state of the STRADalpha pseudokinase and activation of the LKB1 tumour suppressor. *PLoS biology* **7**, e1000126
33. Arteaga, C. L., Ramsey, T. T., Shawver, L. K., and Guyer, C. A. (1997) Unliganded Epidermal Growth Factor Receptor Dimerization Induced by Direct Interaction of Quinazolines with the ATP Binding Site. *Journal of Biological Chemistry* **272**, 23247-23254
34. Bandaranayake, R. M., Ungureanu, D., Shan, Y., Shaw, D. E., Silvennoinen, O., and Hubbard, S. R. (2012) Crystal structures of the JAK2 pseudokinase domain and the pathogenic mutant V617F. *Nat Struct Mol Biol* **19**, 754-759
35. Hu, J., Yu, H., Kornev, A. P., Zhao, J., Filbert, E. L., Taylor, S. S., and Shaw, A. S. (2011) Mutation that blocks ATP binding creates a pseudokinase stabilizing the scaffolding function of kinase suppressor of Ras, CRAF and BRAF. *Proceedings of the National Academy of Sciences of the United States of America* **108**, 6067-6072
36. Lemmon, M. A., Freed, D. M., Schlessinger, J., and Kiyatkin, A. (2016) The Dark Side of Cell Signaling: Positive Roles for Negative Regulators. *Cell* **164**, 1172-1184

37. Wan, P. T. C., Garnett, M. J., Roe, S. M., Lee, S., Niculescu-Duvaz, D., Good, V. M., Project, C. G., Jones, C. M., Marshall, C. J., Springer, C. J., Barford, D., and Marais, R. (2004) Mechanism of Activation of the RAF-ERK Signaling Pathway by Oncogenic Mutations of B-RAF. *Cell* **116**, 855-867
38. McClendon, C. L., Kornev, A. P., Gilson, M. K., and Taylor, S. S. (2014) Dynamic architecture of a protein kinase. *Proc Natl Acad Sci U S A* **111**, E4623-4631
39. Carter, J., Tseng, L.-H., Zheng, G., Dudley, J., Illei, P., Gocke, C. D., Eshleman, J. R., and Lin, M.-T. (2015) Non-p.V600E BRAF Mutations Are Common Using a More Sensitive and Broad Detection Tool. *American Journal of Clinical Pathology* **144**, 620-628
40. Kondo, Y., Ognjenović, J., Banerjee, S., Karandur, D., Merk, A., Kulhanek, K., Wong, K., Roose, J. P., Subramaniam, S., and Kuriyan, J. (2019) Cryo-EM structure of a dimeric B-Raf:14-3-3 complex reveals asymmetry in the active sites of B-Raf kinases. *Science* **366**, 109-115
41. Montagut, C., Sharma, S. V., Shioda, T., McDermott, U., Ulman, M., Ulkus, L. E., Dias-Santagata, D., Stubbs, H., Lee, D. Y., Singh, A., Drew, L., Haber, D. A., and Settleman, J. (2008) Elevated CRAF as a potential mechanism of acquired resistance to BRAF inhibition in melanoma. *Cancer research* **68**, 4853-4861
42. Grasso, M., Estrada, M. A., Ventocilla, C., Samanta, M., Maksimoska, J., Villanueva, J., Winkler, J. D., and Marmorstein, R. (2016) Chemically Linked Vemurafenib Inhibitors Promote an Inactive BRAF(V600E) Conformation. *ACS Chem Biol* **11**, 2876-2888
43. Maier, J. A., Martinez, C., Kasavajhala, K., Wickstrom, L., Hauser, K. E., and Simmerling, C. (2015) ff14SB: Improving the Accuracy of Protein Side Chain and Backbone Parameters from ff99SB. *Journal of chemical theory and computation* **11**, 3696-3713
44. D.A. Case, R. M. B., D.S. Cerutti, T.E. Cheatham, III, T.A. Darden, R.E. Duke, T.J. Giese, H. Gohlke, A.W. Goetz, N. Homeyer, S. Izadi, P. Janowski, J. Kaus, A. Kovalenko, T.S. Lee, S. LeGrand, P. Li, C. Lin, T. Luchko, R. Luo, B. Madej, D. Mermelstein, K.M. Merz, G. Monard, H. Nguyen, H.T. Nguyen, I. Omelyan, A. Onufriev, D.R. Roe, A. Roitberg, C. Sagui, C.L. Simmerling, W.M. Botello-Smith, J. Swails, R.C. Walker, J. Wang, R.M. Wolf, X. Wu, L. Xiao and P.A. Kollman. (2016) Amber 2016.

Table 1. Secondary Structure Analysis of the Activation Loop

	BRAF^{WT} monomer		BRAF^{D594G} monomer[a]		BRAF^{WT} dimer[b]	
Residue	**3_{10} helix**	**α helix**	**3_{10} helix**	**α helix**	**3_{10} helix**	**α helix**
A598	0.000	0.975	0.637	0.000	0.000	0.000
T599	0.000	0.975	0.637	0.000	0.000	0.000
V600	0.006	0.986	0.637	0.000	0.000	0.000
K601	0.008	0.986	0.009	0.000	0.000	0.000
S602	0.142	0.584	0.008	0.000	0.000	0.000
R603	0.142	0.445	0.008	0.000	0.008	0.000
W604	0.138	0.011	0.008	0.000	0.010	0.000

[a] analysis done on trajectory > 240ns (i.e. > 4800 in Figure above)
[b] result of protomer A is shown, result of protomer B is almost identical to A

Table 2. Strength of Key Hydrogen Bond Interactions

H-bond Donor[a]	H-bond Acceptor[a]	WT BRAF dimer	CRAF-BRAF^{D594G}	CRAF dimer
A-R509[b]	B-T508/R506/L505	1.51	1.60	0.00
B-R509	A-T508/R506/L505	1.69	1.66	0.00
A-R509	B-F516	0.69	0.98	0.00
B-R509	A-F516	0.12	0.00	0.99
A-H510	B-H477	0.84	0.84	0.32
B-H510	A-H477	0.97	0.95	0.00
A-R506	B-D448	0.00	2.00	0.00
B-R506	A-D448	1.33	0.00	0.00
Average Number of H-bonds		7.15	8.03	1.31

[a] H-bond donors are guanidino NH in ARG or NH in HIS, H-bond acceptors are carbonyl Os, or carboxylate Os in D448
[b] BRAF(CRAF) residue ID equivalency: R509(R401), T508/R506/L505 (T400/R398/L397), H510(H402), H477(H369), D448(Y340)

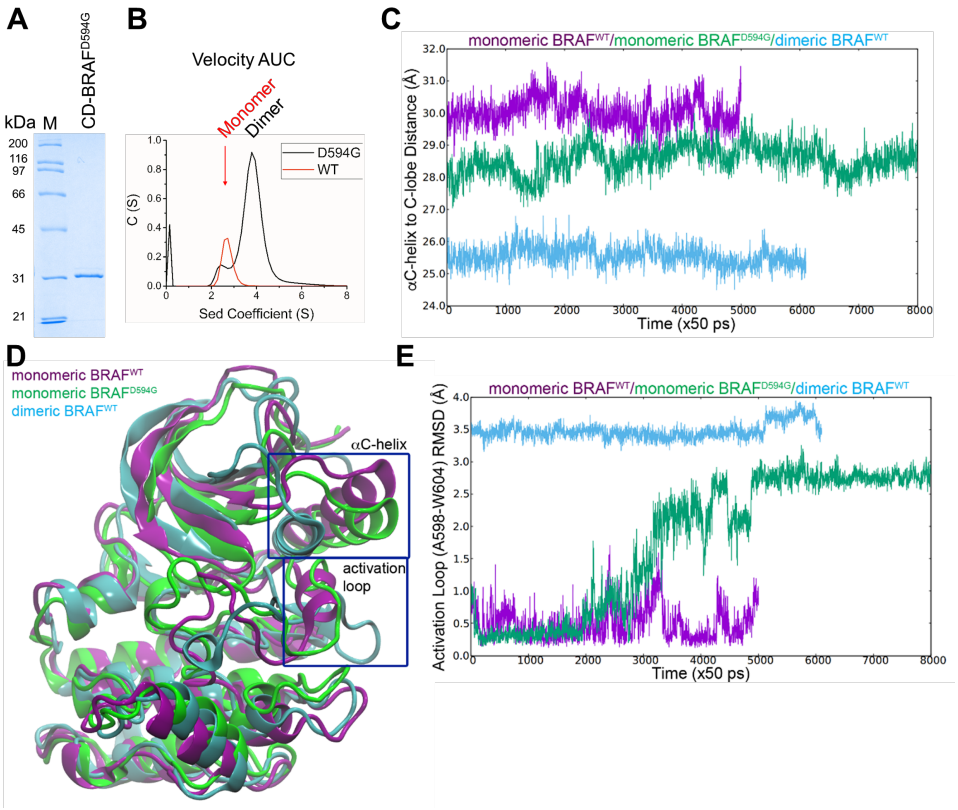

Figure 1: Catalytic Domain of BRAF^{D594G} has Increased Dimerization in Solution as Compared to Its Wild-Type Counterpart. A) CD-BRAF^{D594G} was purified and analyzed by coomassie-blue stained SDS-PAGE. The molecular weight marker (M) and CD-BRAF^{D594G} are identified above the gel. **B)** Purified CD-BRAF^{D594G} and wild-type (WT) CD-BRAF were investigated using velocity AUC. Monomeric BRAF or dimeric BRAF are labeled above the image at ~ 2.5 or ~4 S respectively. **C)** Molecular dynamics trajectory signifying the center of mass distance from the αC-helix towards the C-lobe as a function of simulation time are shown for monomeric WT CD-BRAF (violet), monomeric CD-BRAF^{D594G} (green), and dimeric WT CD-BRAF (blue). **D)** Overlay of the representative snapshot from the MD simulations for monomeric WT CD-BRAF (violet), CD-BRAF^{D594G} (green), and dimeric WT CD-BRAF (blue). The αC-helix and activation loop are highlighted with dark blue boxes. **E)** The stability of the activation loop for monomeric WT CD-BRAF, CD-BRAF^{D594G}, and dimeric WT CD-BRAF was measured by looking at the RMSD (root mean square deviation), with the respect to the average structure of monomeric WT CD-BRAF (featuring the AS-H1 helix throughout the whole trajectory).

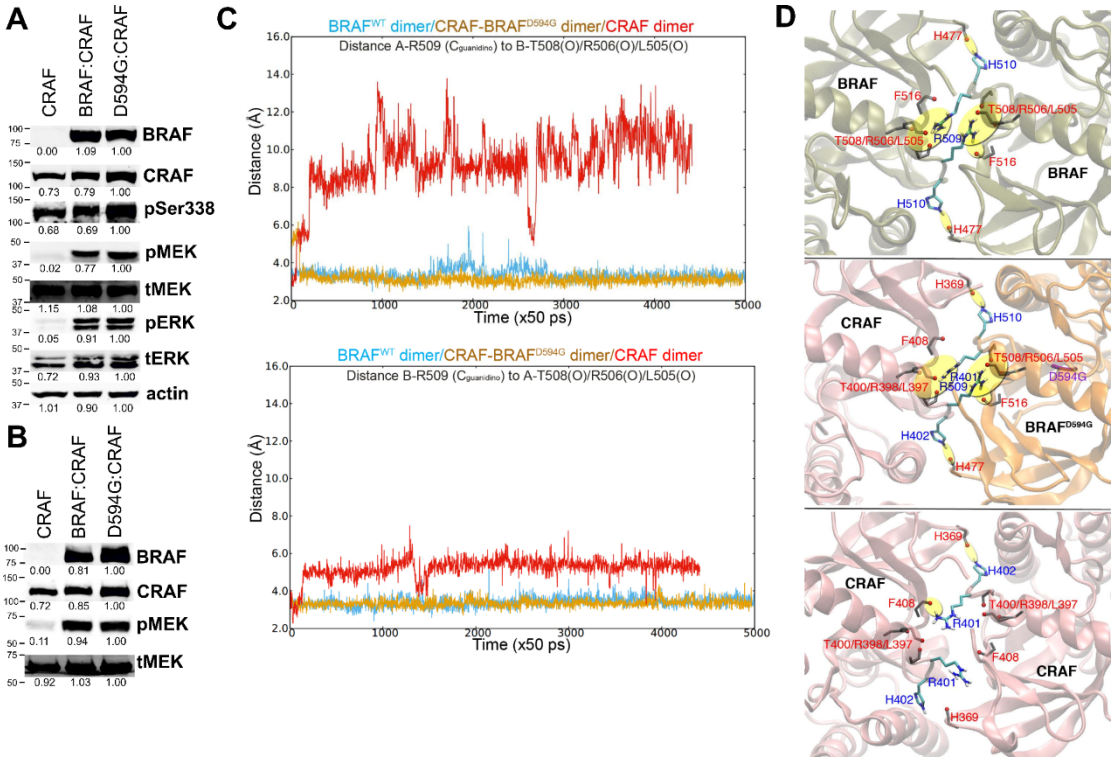

Figure 2: Heterodimers have Stronger Dimer Interfaces than Homodimers. A) CRAF, BRAF:CRAF, and D594G:CRAF were transiently transfected into HEK293 cells and the lysates were probed for the indicated proteins using immunoblotting. **B)** CRAF, BRAF:CRAF, and D594G:CRAF co-immunoprecipitated from cell lysates were incubated with purified MEK1^{K97M} to measure their respective activities by probing for phospho-MEK (pMEK). The western blots are a representative of three independent replicates. The relative intensity values were calculated in ImageJ and are shown below the blot. The molecular weight values (kDa) above and below the band are indicated to the left of the blot. **C)** Molecular dynamics trajectory measuring the distance between the conserved Arg residue's guanidino C (BRAF:R509/CRAF:R401) and the center of a H-bonding acceptors pocket on the other protomer across the dimer interface BRAF:BRAF (blue), CRAF:D594G (gold), and CRAF:CRAF (red). H-bonding from protomer A to protomer B is shown on top, while protomer B to A is shown below. **D)** Representative snapshots of the dimer interfaces of BRAF:BRAF (gray:gray, top), CRAF:D594G (pink:gold, middle), and CRAF:CRAF (pink:pink, bottom). The key hydrogen bond contacts are emphasized with yellow highlights.

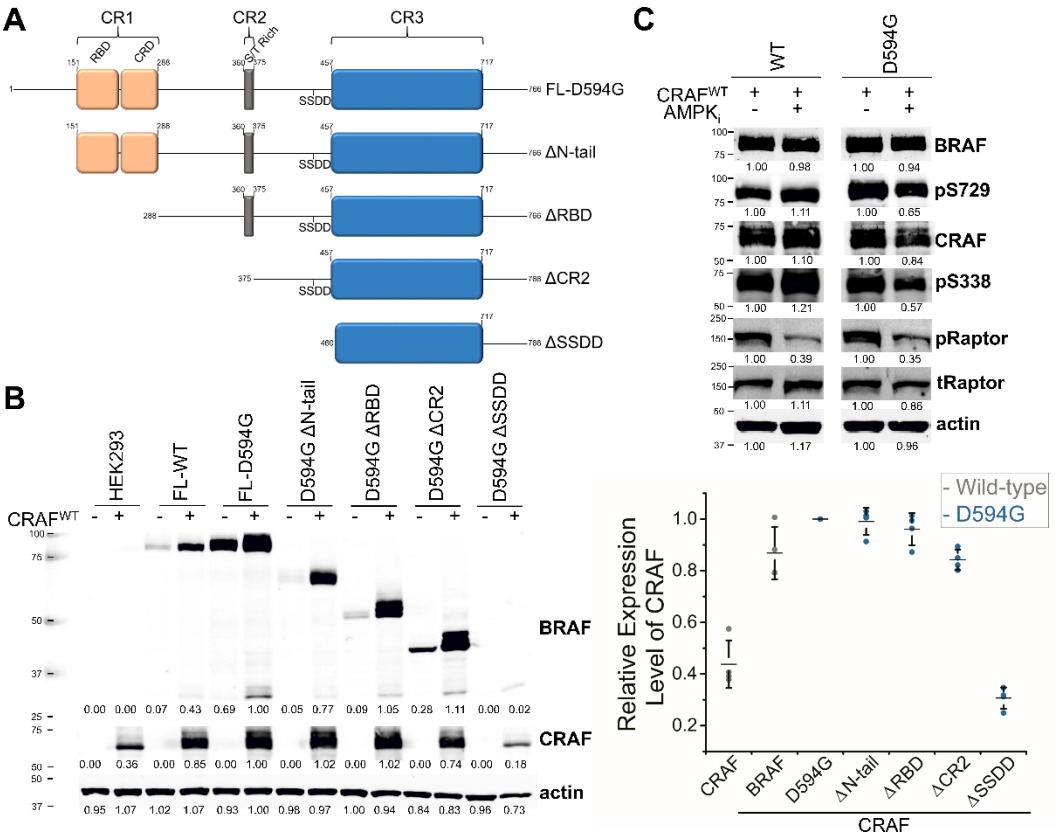

Figure 3: The Stability of BRAF^{D594G} and CRAF is Dependent on Heterodimerization. A) The schematic diagram of the deletion mutants of BRAF^{D594G}. In FL-D594G, the conserved regions (CR1-3) and specific motifs are labeled. The amino acid numbers are identified for the beginning/end of the construct and conserved regions. The RBD (RAS-binding domain), CRD (cysteine rich domain), S/T Rich (Serine/Threonine Rich domain), SSDD (aa. 446-449), and kinase domain are labeled accordingly. **B)** The indicated constructs were transiently transfected into HEK293 cells. We examined the expression changes of D594G in the presence and absence of CRAF in cells cultured under 10% FBS. A scatter plot is shown with the individual points and the average ± S.D. The relative expression level of CRAF indicates CRAF expression alone or in the presence of WT BRAF or D594G constructs which are all normalized to FL-BRAF^{D594G}. **C)** 5 μM of CompoundC, an AMPK inhibitor (AMPK$_i$), was added to HEK293 cells expressing either BRAF:CRAF or D594G:CRAF for 4 h. ImageJ was used to calculate the relative intensity values and are shown below the blot. The molecular weight values (kDa) are shown to the left of the blot.

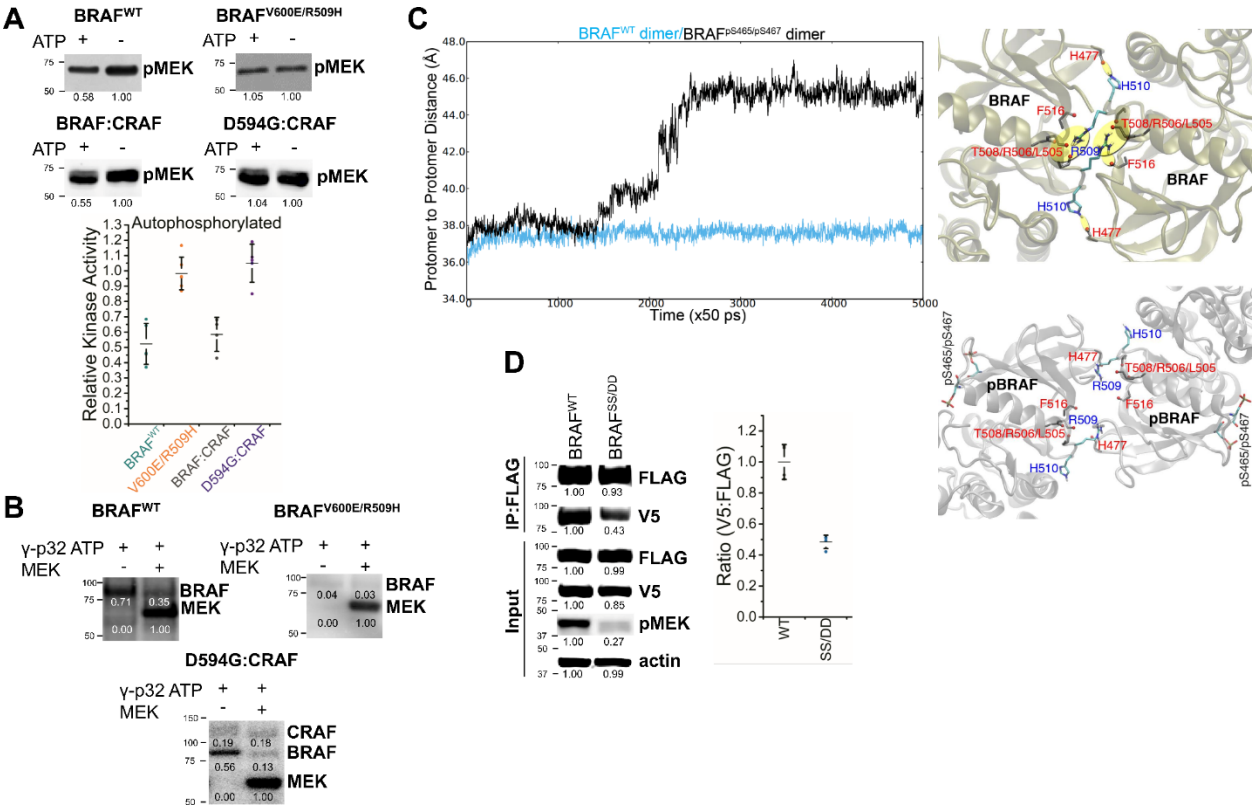

Figure 4: Inhibitory Autophosphorylation of the P-loop Disrupts Dimerization of Wild-Type BRAF and is Bypassed by BRAF^{D594G}:CRAF Heterodimers. A) WT BRAF, BRAF$^{V600E/R509H}$, BRAF:CRAF, and D594G:CRAF were pre-incubated with ATP (+) or without ATP (-) for 30 min at room temperature to allow the completion of autophosphorylation, then were incubated with MEK1^{K97M} for 10 min at 30°C. The relative kinase activities of unphosphorylated RAF protein (Native) and autophosphorylated RAF protein (Auto) were quantified, to the respective native lane of three independent experiments ± S.D., and are shown below the immunoblots. A scatter plot is shown of the relative kinase activity of the autophosphorylated lanes normalized to the respective native lane. **B)** ^{32}P labeled ATP was incubated with wild-type BRAF, BRAF$^{V600E/R509H}$, and D594G:CRAF in the presence and absence of MEK1^{K97M} for 30 min before being subjected to SDS-PAGE radiograph gel imaging. Autophosphorylation of RAF and phosphorylation of MEK1^{K97M} were recorded simultaneously. **C)** Molecular dynamics simulations monitoring the protomer distance of wild-type BRAF or p-loop phosphorylated BRAF (pSer465/pSer467) were examined. The trajectory of the dimer-interface was tracked for wild-type BRAF (blue) and pSer465/pSer467-BRAF (black). Snapshots showing the dimer-interface for wild-type BRAF (Upper) and pSer465/pSer467-BRAF (Lower) are shown to the right. Hydrogen bonding interactions are indicated by yellow circles. **D)** WT BRAF (BRAF^{WT}) and BRAF S465D/S467D (BRAF$^{SS/DD}$) were transiently transfected into HEK293 cells. Flag-tagged BRAF was co-immunoprecipatated from the cell lysate and then probed for V5-tagged BRAF. The ratio of V5 to FLAG is shown to the right of the immunoblots for three independent experiments ± S.D. The relative intensity values are below the blot. The molecular weight standard values (kDa) are identified to the left of the blot.

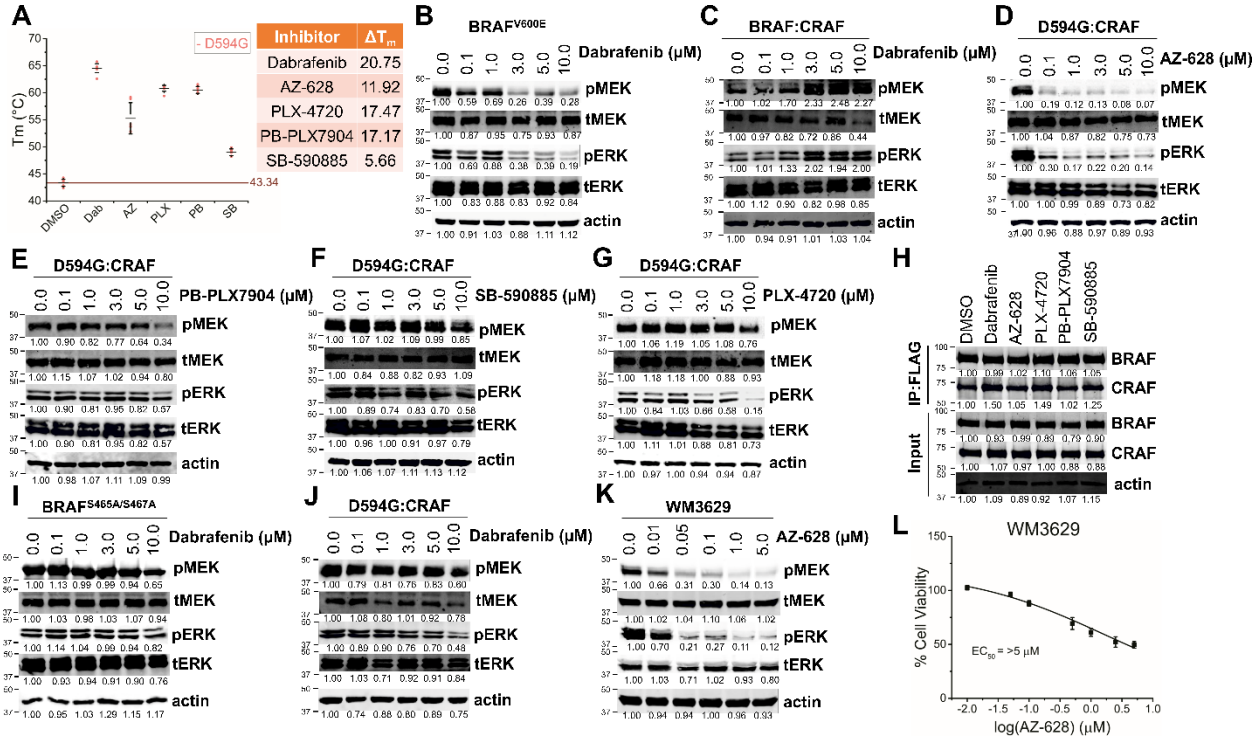

Figure 5: Targeting BRAF^{D594G}:CRAF Heterodimers with ATP-Competitive Inhibitors Displays Drug Resistance Despite of Decreased MAPK Signaling. A) 5 μM of CD-D594G was incubated with 25 μM inhibitor then subjected to DSF. The melting temperature (T_m) of CD-D594G with DMSO, Dabrafenib, AZ-628, PLX-4720, PB-PLX7904, and SB-590885 were plotted. The ΔT_m was calculated by subtracting CD-D594G in the presence of drug minus no treatment. **B-G)** The respective constructs were transiently transfected into HEK293 cells and treated with inhibitor at the indicated drug concentrations for 1 h. **B&C)** BRAF^{V600E} and BRAF:CRAF were treated with dabrafenib. **D-G)** D594G:CRAF was treated with AZ-628 (D), PB-PLX7904 (E), SB-590885 (F)**,** and PLX-4720 (G). **H)** D594G:CRAF was treated with the specified drug for 1 h before lysing then co-immunoprecipitation with anti-FLAG resin. **I&J)** BRAF^{S465AS467A} (I) and D594G:CRAF (J) were treated with dabrafenib in HEK293 cells. **K&L)** Melanoma cells, WM3629, expressing BRAF^{D594G} and NRAS^{G12D} were treated with AZ-628 for 1 h for Western blot analysis (K) or 96 h for cell viability experiments (L). Cell viability was calculated by dividing the A450 (absorbance for the WST reagent) with AZ-628 treatment by the A450 for no treatment x100. The cells were harvested and lysed with 4% SDS then subjected to Western blot analyses, unless otherwise indicated. The relative intensities are underneath the blot. The molecular weight numbers (kDa) are identified to the left of the blot.

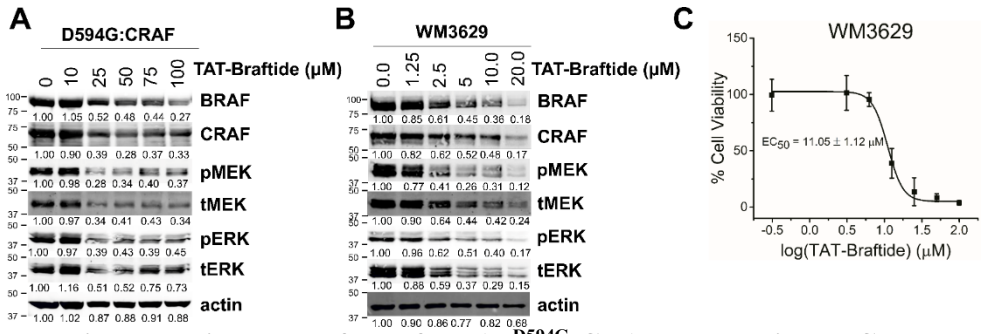

Figure 6: Targeting the Dimer-Interface of BRAF^{D594G}:CRAF Heterodimers Causes Both Protein Degradation and Diminished MAPK Signaling in Cells. A) D594G:CRAF were transiently transfected then treated with TAT-Braftide (0, 10, 25, 50, 75, and 100 μM) for 4 h. **B)** Melanoma cells, WM3629, harboring BRAF^{D594G} and NRAS^{G12D} were treated with TAT-Braftide for 4 h. The cells were harvested and lysed with 4% SDS then subjected to Western blot analyses. **C)** WM3629 were treated with TAT-Braftide for 48 h then the media was replaced with WST reagent diluted in opti-MEM. % Cell Viability was calculated by dividing the A450 with Braftide by the A450 for no treatment x100. The relative intensities of the bands are located below the blot. The molecular weight values (kDa) are located to the left of the blot.

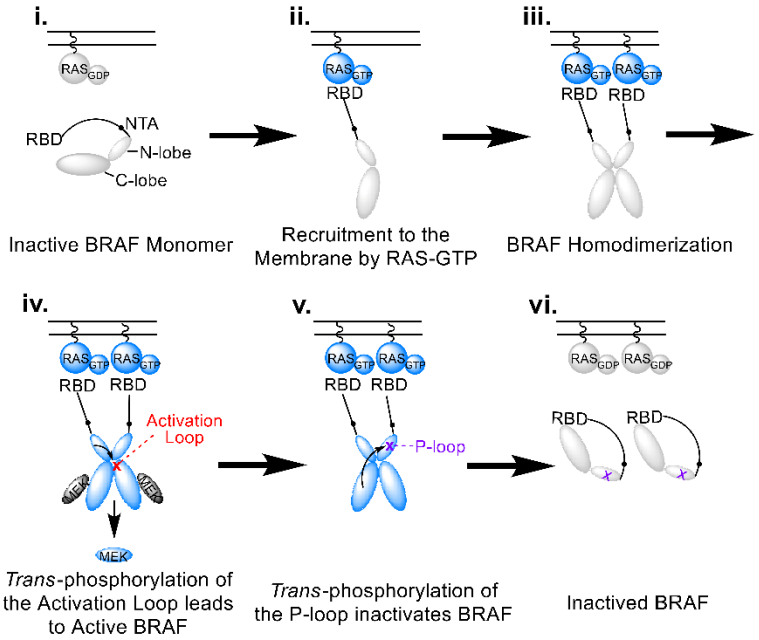

Figure 7: Stepwise activation of BRAF under Physiological Conditions. i) Monomeric BRAF is found in the cytosol with the N-terminal and C-terminal interacting causing BRAF to be inactive. ii) Active RAS stimulates the N-terminal domain of BRAF to release from the C-terminal domain. iii) RAS clustering brings RAF monomers in close proximity which promotes RAF dimerization. iv) BRAF is stabilized by MEK that helps facilitate auto-phosphorylation of the activation loop (red). After MEK phosphorylation, BRAF and MEK dissociate allowing active MEK to interact with ERK. v) BRAF regulates it's activity by auto-phosphorylating the p-loop (Ser465/Ser467 violet) leading to inactive BRAF. vi) P-loop phosphorylation renders BRAF inactive down-regulating the entire MAPK signaling cascade. The inactive kinases are shown in grey while the active kinases are indicated by blue. RAS-binding domain (RBD) and N-terminal acidic (NTA).

Analyses of the oncogenic BRAF^{D594G} variant reveal a kinase-independent function of BRAF in activating MAPK signaling

Nicholas J. Cope, Borna Novak, Zhiwei Liu, Maria Cavallo, Amber Y. Gunderwala, Matthew Connolly and Zhihong Wang

J. Biol. Chem. published online January 12, 2020
